

Factorization of event-plane correlations over transverse momentum in relativistic heavy ion collisions in a multi-phase transport model

Kai Xiao,^{1,*} Feng Liu,^{2,†} and Fuqiang Wang^{2,3,‡}

¹*College of Electronics and Information Engineering,
South-Central University for Nationalities, Wuhan 430074, China*

²*Key Laboratory of Quark and Lepton Physics (MOE) and Institute of Particle Physics,
Central China Normal University, Wuhan 430079, China*

³*Department of Physics, Purdue University, West Lafayette, Indiana 47907, USA*

(Dated: August 20, 2021)

Momentum-space azimuthal harmonic event planes (EP) are constructed from final-state mid-rapidity particles binned in transverse momentum (p_T) in $\sqrt{s_{NN}} = 200$ GeV Au+Au collisions in a multi-phase transport (AMPT) model. The EP correlations between p_T bins, corrected by EP resolutions, are smaller than unity. This indicates that the EP's decorrelate over p_T in AMPT, qualitatively consistent with data and hydrodynamic calculations. It is further found that the EP correlations approximately factorize into single p_T -bin EP correlations to a common plane. This common plane appears to be the momentum-space EP integrated over all p_T , not the configuration-space participant plane (PP).

PACS numbers: 25.75.Ld, 25.75.Dw, 24.10.Jv, 24.10.Lx

I. INTRODUCTION

In high energy heavy ion collisions, the initial high energy density and pressure buildup drive the collision system to rapid expansion. In non-central collisions, the pressure gradient is anisotropic due to the anisotropic transverse overlap geometry, resulting in an observable momentum-space azimuthal anisotropy [1]. The particle azimuthal distribution can be expressed in Fourier series:

$$\frac{d^2 N}{dp_T d\phi} \propto 1 + \sum 2v_n \cos[n(\phi - \Psi_n)], \quad (1)$$

where ϕ represents the particle azimuthal angle and Ψ_n is the n^{th} harmonic plane angle. The Fourier coefficients [2]

$$v_n = \langle \cos[n(\phi - \Psi_n)] \rangle, \quad (2)$$

characterize the magnitudes of the harmonic anisotropies, where the bracket $\langle \dots \rangle$ denotes averages over particles and events. In the limit of smooth nuclei, odd harmonics vanish; Ψ_2 coincides with the reaction plane (the plane defined by the beam direction and the impact parameter vector), and elliptic flow (v_2) is the leading component because of the predominant elliptic overlap shape. Large v_2 has been measured experimentally [3]. In fact, the measured v_2 is so large that hydrodynamic descriptions are applicable, and a

very small shear viscosity to entropy density ratio (η/s) is required [4]. This constitutes an important evidence for the formation of a new form of matter, the strongly interacting quark-gluon plasma (sQGP) in relativistic heavy ion collisions [3]. Due to fluctuations, the energy density in the overlap region is lumpy, so all harmonics can exist [5] and the harmonic planes of different orders are unnecessarily the same. Higher order harmonics are more sensitive to η/s , and hence play an important role in extracting precise information about the sQGP medium [6].

As the initial configuration space information of the overlap region is not experimentally accessible, the harmonic symmetry plane Ψ_n^{PP} in configuration space, called the participant plane (PP), cannot be measured. In experiment, anisotropic flow is measured via final-state particle correlations [3]. For example, one constructs an event plane (EP), Ψ_n^{EP} , by the final-state particle momenta, as a proxy for Ψ_n^{PP} [7]. One then correlates a test particle with the Ψ_n^{EP} to measure anisotropic flow via Eq.(2) where the deviation of Ψ_n^{EP} from Ψ_n is corrected by a resolution factor [7]. Alternatively, the anisotropic flow is measured using azimuthal correlations between the observed particles, where the Fourier coefficients of the correlation function are given by

$$V_n(p_T^a, p_T^b) \equiv \langle \cos[n(\phi^a - \phi^b)] \rangle. \quad (3)$$

Often factorization is assumed where the two-particle correlations arise only from the single particle correlations to a common harmonic plane Ψ_n (i.e. nonflow intrinsic particle correlations are neglected). Under such conditions, since the common Ψ_n cancel in $(\phi^a - \Psi_n) - (\phi^b - \Psi_n)$, one has

*Electronic address: kxiao@mails.cnu.edu.cn

†Electronic address: fliu@mail.cnu.edu.cn

‡Electronic address: fqwang@purdue.edu

$$V_n(p_T^a, p_T^b) = v_n(p_T^a)v_n(p_T^b). \quad (4)$$

The single-particle anisotropic flow v_n can be simply obtained as the square root of the two-particle cumulant measurement in Eq.(3) by choosing the two particles from the same phase space, or when the v_n of one particle is known (referred to as the reference particle).

Studies have shown, however, that the harmonic planes, whether in configuration or momentum space, are not the same at different pseudorapidities. Previous works [8, 9] have shown that EP's are decorrelated over pseudorapidity (η) and the decorrelation increases with increasing η gap between the two particles.

Not only does the harmonic plane depend on η , but also on transverse momentum (p_T). Gardim et al. [10] have pointed out with ideal hydrodynamic calculations that the fluctuating flow angles Ψ_n depend on p_T . Viscous hydrodynamic calculations [11] indicate that the harmonic planes decorrelate over p_T even in the same η region. This is indeed observed by CMS in Pb+Pb and p+Pb collisions at the LHC [12]. The experimental confirmation of the p_T decorrelation is taken as a strong evidence supporting hydrodynamic descriptions of relativistic heavy ion collisions.

Experimentally, in order to reduce nonflow correlations (such as small angle jet correlations and resonance decays), one often apply η gap between the two particles used in correlation measurements. In measuring high p_T particle anisotropy, the reference particle is often taken at low p_T . The harmonic plane decorrelation over η and p_T casts a problem in those measurements; it may require the EP to be constructed in the same phase space as the particle of interest in order to measure flow anisotropy [9]. As an operational definition, one may define the flow of particles in a particular phase space as that with respect to the harmonic plane of the same phase space region. Namely,

$$v_n(\eta, p_T) = \langle \cos[n(\phi(\eta, p_T) - \Psi_n(\eta, p_T))] \rangle. \quad (5)$$

We note, however, that such v_n is, in reality, contaminated by non-negligible nonflow effects.

The η and p_T decorrelation of the harmonic planes explicitly breaks factorization of Eq.(4). This is easy to see. The two-particle cumulant measurement with the two particles coming from different phase spaces is

$$\begin{aligned} V_n(p_T^a, p_T^b) &\equiv \langle \cos[n(\phi_n(p_T^a) - \phi_n(p_T^b))] \rangle \\ &= v_n(p_T^a)v_n(p_T^b) \cos[n(\Psi_n(p_T^a) - \Psi_n(p_T^b))]. \end{aligned} \quad (6)$$

The two harmonic planes from different phase spaces are now different and can no longer cancel in two-particle azimuthal correlations. Note that in Eq.(6) we have neglected possible nonflow contributions (which is usually

small when a large phase-space gap is imposed between the two particles), so that we can write the average of the product into the product of averages.

The EP decorrelations were experimentally measured to be appreciable [12]. However, the experimentally measured two-particle cumulants obey factorization exceedingly well [13]. It implies that $\cos[n(\Psi_n(p_T^a) - \Psi_n(p_T^b))]$ correlations between two phase spaces, a and b , must factorize to a good degree [14]. This is by no means obvious.

In this paper we try to address two questions. One, are EP's in parton transport model similarly decorrelated as in data and hydrodynamic calculations? Second, how well are the EP correlations factorized? The answers to these questions can hopefully reveal additional insights to the physics of EP decorrelations.

II. ANALYSIS METHOD

The AMPT (A Multi-Phase Transport) model with string melting describes many experimental data reasonably well, particularly the anisotropic flow measurements [15]. We thus use the AMPT model with string melting for our study. There are four main components in AMPT: the initial conditions, parton interactions, hadronization, and hadron interactions. The initial conditions are obtained from the HIJING model [16], which includes the spatial and momentum information of minijet partons from hard processes and strings from soft processes. The time evolution of partons is then treated according to the ZPC parton cascade model [17]. After parton interactions cease, a combined coalescence and string fragmentation model is used for the hadronization of partons. The scattering among the resulting hadrons is described by a relativistic transport (ART) model [18] which includes baryon-baryon, baryon-meson and meson-meson elastic, and inelastic scatterings.

In AMPT model, two harmonic planes can be constructed. One is calculated from the initial configuration space information of partons by [5]

$$\Psi_n^{PP} = \frac{\text{atan2}(\langle r^n \sin(n\phi_r) \rangle, \langle r^n \cos(n\phi_r) \rangle) + \pi}{n}, \quad (7)$$

where r and ϕ_r are the polar coordinate position of each parton. Because of event-by-event geometry fluctuations, Ψ_n^{PP} is not necessarily as same as the reaction plane. Experimentally, the coordinate space information is not accessible. Instead, the EP can be constructed from final-state particle momenta by

$$\Psi_n^{EP} = \frac{\text{atan2}(\langle \sin(n\phi) \rangle, \langle \cos(n\phi) \rangle)}{n}, \quad (8)$$

where ϕ is the azimuthal angle of the particle momentum. Due to the finite multiplicity of constituents, the constructed harmonic plane is smeared from the true one, Ψ_n^{true} —the geometry harmonic plane of the participant

p_T (GeV/c)	$n = 2$	$n = 3$	p_T (GeV/c)	$n = 2$	$n = 3$
0 – 0.2	0.11 ± 0.03	0.06 ± 0.04	0.2 – 2.0	0.889 ± 0.001	0.568 ± 0.004
0.2 – 0.4	0.557 ± 0.005	0.17 ± 0.02	0 – 0.2 0.4 – 2.0	0.853 ± 0.002	0.537 ± 0.004
0.4 – 0.6	0.719 ± 0.003	0.339 ± 0.008	0 – 0.4 0.6 – 2.0	0.810 ± 0.002	0.435 ± 0.006
0.6 – 0.8	0.684 ± 0.003	0.384 ± 0.007	0 – 0.6 0.8 – 2.0	0.829 ± 0.002	0.435 ± 0.006
0.8 – 1.0	0.608 ± 0.004	0.364 ± 0.007	0 – 0.8 1.0 – 2.0	0.847 ± 0.002	0.462 ± 0.005
1.0 – 1.2	0.525 ± 0.006	0.313 ± 0.009	0 – 1.0 1.2 – 2.0	0.858 ± 0.001	0.480 ± 0.005
1.2 – 1.4	0.423 ± 0.008	0.26 ± 0.01	0 – 1.2 1.4 – 2.0	0.864 ± 0.001	0.496 ± 0.005
1.4 – 1.6	0.36 ± 0.01	0.23 ± 0.01	0 – 1.4 1.6 – 2.0	0.866 ± 0.001	0.506 ± 0.005
1.6 – 1.8	0.32 ± 0.01	0.21 ± 0.01	0 – 1.6 1.8 – 2.0	0.867 ± 0.001	0.507 ± 0.005
1.8 – 2.0	0.33 ± 0.01	0.23 ± 0.01	0 – 1.8	0.867 ± 0.001	0.507 ± 0.005

TABLE I: (Color online) The resolutions, \mathfrak{R}_n^{EP} of the second- and third-order harmonic EP's constructed by final-state particle momentum azimuthal angles in different transverse momentum (p_T) bins. Particles are taken from pseudo-rapidity range of $|\eta| < 1.0$ in 20-40% centrality ($b = 6.79$ - 9.61 fm) Au+Au collisions at $\sqrt{s_{NN}} = 200$ GeV simulated by the AMPT model (string melting, 3 mb parton cross section).

$p_T^a \backslash p_T^b$	0 – 0.2	0.2 – 0.4	0.4 – 0.6	0.6 – 0.8	0.8 – 1.0	1.0 – 1.2	1.2 – 1.4	1.4 – 1.6	1.6 – 1.8	1.8 – 2.0
1.8 – 2.0	-0.32 ± 0.38	0.79 ± 0.14	0.70 ± 0.07	0.82 ± 0.06	0.86 ± 0.07	0.92 ± 0.08	0.90 ± 0.09	0.70 ± 0.12	0.65 ± 0.12	
1.6 – 1.8	-0.43 ± 0.43	0.85 ± 0.16	0.87 ± 0.08	0.91 ± 0.07	0.77 ± 0.08	0.92 ± 0.09	0.81 ± 0.11	0.98 ± 0.13		0.86 ± 0.05
1.4 – 1.6	-0.79 ± 0.43	0.51 ± 0.16	1.00 ± 0.08	1.07 ± 0.07	0.98 ± 0.08	1.10 ± 0.09	1.06 ± 0.11		0.94 ± 0.05	0.90 ± 0.05
1.2 – 1.4	0.16 ± 0.34	0.66 ± 0.13	1.00 ± 0.06	1.00 ± 0.06	1.06 ± 0.06	0.87 ± 0.07		0.97 ± 0.04	0.93 ± 0.04	0.92 ± 0.04
1.0 – 1.2	-0.32 ± 0.28	0.88 ± 0.11	0.85 ± 0.05	0.88 ± 0.05	1.03 ± 0.05		1.02 ± 0.02	0.95 ± 0.03	0.88 ± 0.03	0.85 ± 0.03
0.8 – 1.0	-0.32 ± 0.24	0.68 ± 0.09	1.00 ± 0.05	0.88 ± 0.04		0.98 ± 0.02	0.95 ± 0.02	0.97 ± 0.03	0.93 ± 0.03	0.86 ± 0.03
0.6 – 0.8	-1.00 ± 0.23	0.82 ± 0.09	0.88 ± 0.04		0.95 ± 0.01	0.97 ± 0.01	0.96 ± 0.02	0.92 ± 0.02	0.93 ± 0.03	0.89 ± 0.02
0.4 – 0.6	-0.45 ± 0.26	0.76 ± 0.10		0.97 ± 0.01	0.96 ± 0.01	0.95 ± 0.01	0.94 ± 0.02	0.90 ± 0.02	0.91 ± 0.02	0.86 ± 0.02
0.2 – 0.4	0.60 ± 0.51		0.95 ± 0.01	0.94 ± 0.01	0.95 ± 0.02	0.97 ± 0.02	0.93 ± 0.02	0.92 ± 0.03	0.96 ± 0.03	0.87 ± 0.03
0 – 0.2		0.81 ± 0.09	0.97 ± 0.07	0.87 ± 0.08	0.92 ± 0.09	1.06 ± 0.10	1.00 ± 0.12	0.94 ± 0.14	0.99 ± 0.16	0.86 ± 0.16

TABLE II: (Color online) The resolution-corrected EP correlation strengths $C_2(p_T^a, p_T^b)$ (right down corner) and $C_3(p_T^a, p_T^b)$ (left up corner) of Eq.(9) for different combinations of p_T^a and p_T^b ($p_T^a \neq p_T^b$). Particles used in EP construction are restricted within pseudo-rapidity $|\eta| < 1.0$. The data are simulated by AMPT (string melting, 3 mb cross section) in 20-40% centrality ($b = 6.79$ - 9.61 fm) in Au+Au collisions at $\sqrt{s_{NN}} = 200$ GeV.

partons in configuration space in the limit of infinite parton multiplicity– by a resolution factor. The resolution factor $\mathfrak{R}_n = \langle \cos[n(\Psi_n - \Psi_n^{true})] \rangle$ is calculated with an iterative procedure by the sub-event method, dividing the constituents randomly into two sub-events [7]. Because of the large initial parton multiplicity, the calculated initial configuration-space PP resolution, \mathfrak{R}_n^{PP} , is nearly unity [9]. However, the final-state hadron multiplicity is smaller so the final-state momentum-space EP

resolution, \mathfrak{R}_n^{EP} , is smaller than unity. The EP resolutions in different p_T bins are tabulated in Table I for both the second- and third-order harmonic EP's. In addition, the resolutions of the EP's constructed from all particles in $0 < p_T < 2$ GeV/c but excluding those in a particular p_T bin are also listed.

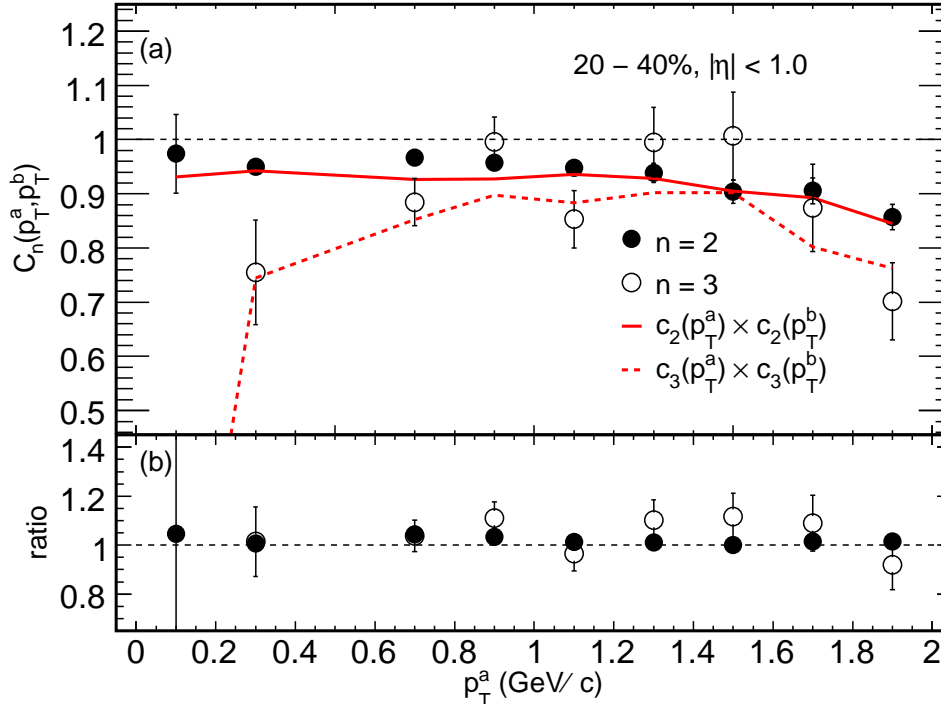


FIG. 1: (Color online) Upper panel shows the EP correlation strength $C_n(p_T^a, p_T^b)$, corrected by the corresponding EP resolutions, as a function of p_T^a for a fixed p_T^b bin. Particles used in EP construction are restricted within pseudo-rapidity $|\eta| < 1.0$. The data are simulated by AMPT (string melting, 3 mb cross section) in 20-40% centrality ($b = 6.79$ - 9.61 fm) in Au+Au collisions at $\sqrt{s_{NN}} = 200$ GeV. Red lines are the fit to data by the function of $c_n(p_T^a) \times c_n(p_T^b)$ where $c_n(p_T)$ is a set of ten fit parameters. Lower panel shows the ratio of the data points to the fit result.

III. RESULTS AND DISCUSSIONS

The EP angles $\Psi_n^{EP}(p_T)$ are constructed from final-state charged particle momenta in ten equal-width p_T bins in $0 < p_T < 2$ GeV/c. Particles used in the EP construction are restricted within $|\eta| < 1.0$. Both the elliptic ($n = 2$) and triangular ($n = 3$) EP's are constructed. The EP correlation between p_T^a and p_T^b bins, corrected by the EP resolutions in Table I, is given by:

$$C_n(p_T^a, p_T^b) = \frac{\langle \cos[n(\Psi_n^{EP}(p_T^a) - \Psi_n^{EP}(p_T^b))] \rangle}{\Re_n^{EP}(p_T^a) \Re_n^{EP}(p_T^b)}. \quad (9)$$

The EP correlation strengths C_n are tabulated in Table II for both $n = 2$ and $n = 3$. For each $C_n(p_T^a, p_T^b)$ value in the table, we have already taken the average of $C_n(p_T^a, p_T^b)$ and $C_n(p_T^b, p_T^a)$. As seen from the table, the measured $C_n(p_T^a, p_T^b)$ for $p_T^a \neq p_T^b$ are less than unity. This indicates that the EP's in AMPT are indeed decorrelated over p_T . The decorrelations are similar in magnitude to those observed in data at the LHC [12] and from hydrodynamic calculations [11]. Figure 1(a) shows the EP correlation strengths C_n as a function of p_T^a for a fixed $p_T^b = 0.4 < p_T < 0.6$ GeV/c, as an example.

To test factorizability, the EP correlations of all combinations of p_T^a and p_T^b are fitted by a set of ten parameter $c_n(p_T)$ corresponding to the ten p_T bins:

$$C_n(p_T^a, p_T^b) = c_n(p_T^a) \times c_n(p_T^b). \quad (10)$$

Factorization of the EP correlations can be tested by the fitting quality. The fit result, $c_n(p_T^a) \times c_n(p_T^b)$, is shown as the curves in Fig.1 along with the EP correlations data points from AMPT, $C_n(p_T^a, p_T^b)$. Fits are good for both $n=2$ and $n=3$. To illustrate the fit quality, Fig. 1(b) shows the ratio of the AMPT data to the fit. The ratio is consistent with unity. Note Fig.1 is only a subset of the EP correlation data for a fixed p_T^b bin as an example, but all $10 \times 9/2$ correlation data for a given harmonic ($n = 2$ or 3) are fitted simultaneously with ten fit parameters in a single fit. The fit χ^2/ndf are 30.5/35 and 45.5/35 for C_2 and C_3 , respectively. Our fit results indicate that the EP correlations are well factorized. The EP correlation between two p_T bins is determined by only the properties of the two single- p_T bins. This may indicate that the EP decorrelation is of a random nature.

Since $C_n(p_T^a, p_T^b)$ factorize well into products of single p_T -bin EP quantities, the fit results suggest that the EP correlations may be caused by single p_T -bin EP correla-

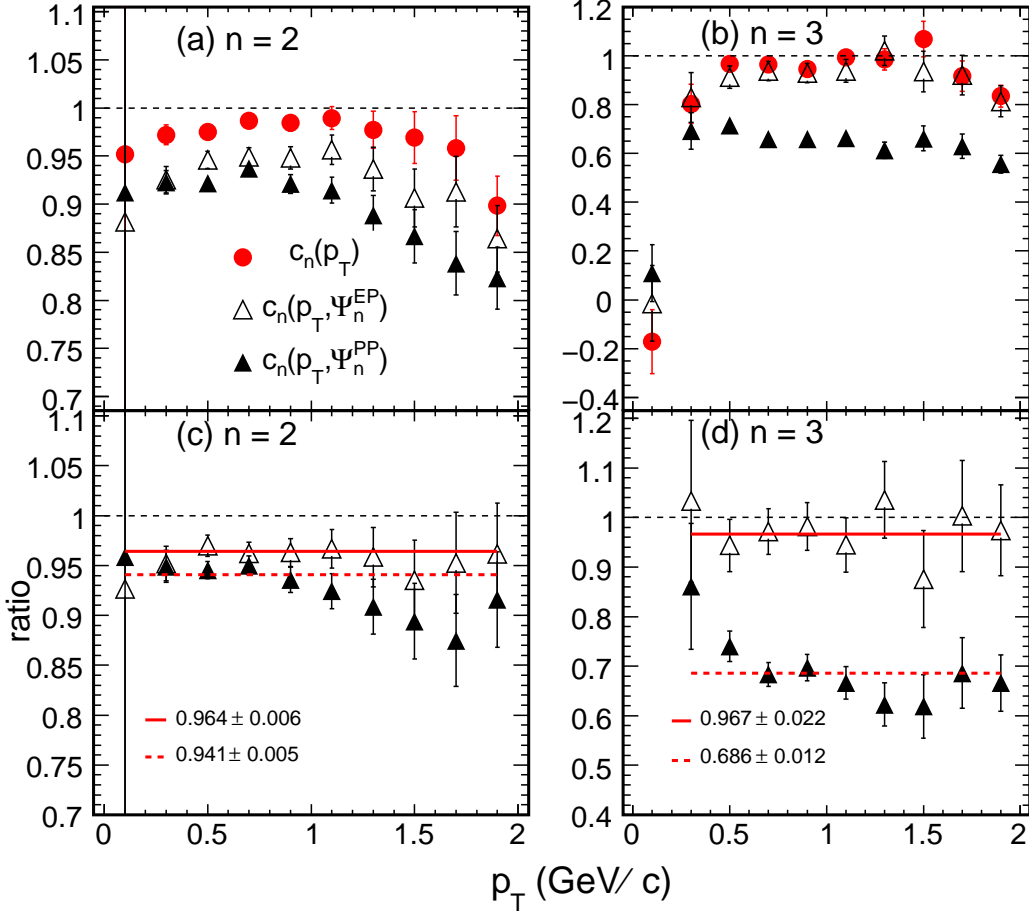


FIG. 2: (Color online) Upper panels show the comparisons of the fit parameter $c_n(p_T)$ to $c_n(p_T, \Psi_n^{EP})$, the correlations between $\Psi_n^{EP}(p_T)$ and the EP constructed from all p_T (but excluding the relevant p_T bin) and $c_n(p_T, \Psi_n^{PP})$, the correlation between $\Psi_n^{EP}(p_T)$ and the PP, for (a) second- and (b) third-order harmonic. Lower panels show the corresponding ratios. Data are for 20-40% centrality ($b = 6.79$ - 9.61 fm) in Au+Au collisions at $\sqrt{s_{NN}} = 200$ GeV from the AMPT model (string melting, 3 mb parton cross section).

tions to a common plane, Ψ_n . Namely,

$$\frac{\langle \cos[n(\Psi_n^{EP}(p_T^a) - \Psi_n^{EP}(p_T^b))] \rangle}{\Re_n^{EP}(p_T^a)\Re_n^{EP}(p_T^b)} = \frac{\langle \cos[n(\Psi_n^{EP}(p_T^a) - \Psi_n)] \rangle}{\Re_n^{EP}(p_T^a)} \times \frac{\langle \cos[n(\Psi_n^{EP}(p_T^b) - \Psi_n)] \rangle}{\Re_n^{EP}(p_T^b)}, \quad (11)$$

and

$$c_n(p_T) = \frac{\langle \cos[n(\Psi_n^{EP}(p_T) - \Psi_n)] \rangle}{\Re_n^{EP}(p_T)}. \quad (12)$$

The good fitting quality demands an answer to the following question: what plane is Ψ_n ? To address this

question, we show in upper panel of Fig. 2 the comparisons between the fit parameter $c_n(p_T)$ and that given by Eq.(12) where Ψ_n is in one case calculated by the configuration-space Ψ_n^{PP} and in the other case by the momentum-space Ψ_n^{EP} from particles over the entire p_T range:

and

$$c_n(p_T, \Psi_n^{PP}) = \frac{\langle \cos[n(\Psi_n^{EP}(p_T) - \Psi_n^{PP})] \rangle}{\mathfrak{R}_n^{EP}(p_T)\mathfrak{R}_n^{PP}} \quad (13)$$

$$c_n(p_T, \Psi_n^{EP}) = \frac{\langle \cos[n(\Psi_n^{EP}(p_T) - \Psi_n^{EP}(0 < p_T < 2 \text{ GeV}/c \text{ but exclude } p_T))] \rangle}{\mathfrak{R}_n^{EP}(p_T)\mathfrak{R}_n^{EP}(0 < p_T < 2 \text{ GeV}/c \text{ but exclude } p_T)} \quad (14)$$

respectively. The Ψ_n^{PP} are constructed from the initial parton configuration within the pseudo-rapidity of $|\eta_{parton}| < 1.0$. The Ψ_n^{EP} are constructed from the final-state particle momenta within $|\eta_{hadron}| < 1.0$ and $0 < p_T < 2 \text{ GeV}/c$ but excluding the p_T bin of interest. To remove auto-correlations, the construction of Ψ_n^{EP} excludes particles of the particular p_T bin used for the construction of $\Psi_n(p_T)$. The resolutions \mathfrak{R}^{PP} and $\mathfrak{R}_n^{EP}(0 < p_T < 2 \text{ GeV}/c \text{ but exclude } p_T)$ are to take into account the inaccuracy of the constructed PP and EP (although \mathfrak{R}^{PP} is found to be approximately unity).

The comparisons of $c_n(p_T)$ to $c_n(p_T, \Psi_n^{PP})$ and $c_n(p_T, \Psi_n^{EP})$ are shown in Fig.2 for both the second- and third-order harmonic EP's. We find that $c_n(p_T, \Psi_n^{EP})$ is more consistent with the fit parameter $c_n(p_T)$ than $c_n(p_T, \Psi_n^{PP})$ is. The more quantitative comparisons are shown in Fig. 2(c) and (d) where the ratios are depicted. The ratio of $c_3(p_T, \Psi_3^{EP})/c_3(p_T)$ is consistent with unity while $c_3(p_T, \Psi_3^{PP})/c_3(p_T)$ is not. For $n = 2$, both ratios are smaller than unity, however, $c_2(p_T, \Psi_2^{EP})/c_2(p_T)$ is closer to unity than $c_2(p_T, \Psi_2^{PP})/c_2(p_T)$. The deviation of $c_2(p_T, \Psi_2^{EP})/c_2(p_T)$ from unity could be due to nonflow effect where some particles are intrinsically correlated in the final-state momentum space. Our results show that the global harmonic plane is not the Ψ_n^{PP} ; it may be the Ψ_n^{EP} . In other words, $\Psi_n^{EP}(p_T)$ fluctuates randomly around Ψ_n^{EP} , not Ψ_n^{PP} .

IV. CONCLUSIONS

In summary, we have studied momentum-space event plane (EP) correlations in $b = 6.79\text{-}9.61 \text{ fm Au+Au}$ collisions at $\sqrt{s_{NN}} = 200 \text{ GeV}$ using the AMPT model (string melting, 3 mb parton cross section). The EP's are constructed from final-state mid-rapidity particles binned in p_T . Both the second- and third-order harmonic EP's are studied. The EP correlations between p_T bins are corrected by the corresponding EP resolutions. The EP correlations are found to be smaller than unity, indicating that the EP's decorrelate over p_T in AMPT, qualitatively consistent with data and hydrodynamic calculations. It is further found that the EP correlations factorize into single p_T -bin EP correlations to a common plane. This common plane appears to be approximately the momentum-space EP integrated over all p_T , but not the configuration-space participant plane (PP).

V. ACKNOWLEDGMENTS

This work is supported in part by MOST of China under 973 Grant 2015CB856901, the National Natural Science Foundation of China under grant No. 11228513, 11221504 and 11135011, U.S. Department of Energy under Grant No. DE-FG02-88ER40412, Fundamental Research Funds for the Central Universities (Grant No. CZQ15001).

[1] J. Y. Ollitrault, Phys. Rev. D **46**, 229 (1992).
 [2] S. Voloshin and Y. Zhang, Z. Phys. C **70**, 665 (1996).
 [3] I. Arsene *et al.* (BRAHMS Collaboration), Nucl. Phys. A **757**, 1 (2005); B. B. Back *et al.* (PHOBOS Collaboration), Nucl. Phys. A **757**, 28 (2005); J. Adams *et al.* (STAR Collaboration), Nucl. Phys. A **757**, 102 (2005); S. S. Adcox *et al.* (PHENIX Collaboration), Nucl. Phys. A **757**, 184 (2005).

[4] P. Romatschke and U. Romatschke, Phys. Rev. Lett. **99**, 172301 (2007); U. Heinz, C. Shen, and H. C. Song, AIP Conf. Proc. **1441**, 766 (2012).
 [5] B. Alver and G. Roland, Phys. Rev. C **81**, 054905 (2010).
 [6] B. H. Alver, C. Gombeaud, M. Luzum, and J. Y. Ollitrault, Phys. Rev. C **82**, 034913 (2010); B. Schenke, S. Jeon, and C. Gale, Phys. Rev. Lett. **106**, 042301 (2011).
 [7] A. M. Poskanzer and S. A. Voloshin, Phys. Rev. C **58**,

- 1671 (1998).
- [8] P. Bozek, W. Broniowski, and J. Moreira, Phys. Rev. C **83**, 034911 (2011); J. Jia and P. Huo, Phys. Rev. C **90**, 034915 (2014).
- [9] K. Xiao, F. Liu, and F. Wang, Phys. Rev. C **87**, 011901(R) (2013).
- [10] F. G. Gardim et al. Phys. Rev. C **87**, 031901(R) (2013).
- [11] U. Heinz, Z. Qiu, and C. Shen, Phys. Rev. C **87**, 034913 (2013).
- [12] S. Chatrchyan *et al.* (CMS Collaboration), JHEP **02**, 088 (2014); V. Khachatryan *et al.* (CMS Collaboration), arXiv:1503.01692v1 (2015).
- [13] B. Alver et al. (PHOBOS Collaboration), Phys. Rev. C **81**, 034915 (2010); K. Aamodt et al. (ALICE Collaboration), Phys. Lett. B **708**, 249 (2012); S. Chatrchyan et al. (CMS Collaboration), Eur. Phys. J. C **72**, 2012 (2012); G. Aad et al. (ATLAS Collaboration), Phys. Rev. C **86**, 014907 (2012).
- [14] F. Wang, Prog. Part. Nucl. Phys., **74**, 35 (2014).
- [15] L. W. Chen, C. M. Ko, and Z. W. Lin, Phys. Rev. C **69**, 031901 (2004).
- [16] X. N. Wang and M. Gyulassy, Phys. Rev. D **44**, 3501 (1991).
- [17] B. Zhang, Comput. Phys. Commun. **109**, 193 (1998).
- [18] B. A. Li and C. M. Ko, Phys. Rev. C **52**, 2037 (1995).